Journal of Visualized Experiments

Spark Plasma Sintering Apparatus used for the Formation of Strontium Titanate Bicrystals

--Manuscript Draft--

Manuscript Number:	JoVE55223R1
Full Title:	Spark Plasma Sintering Apparatus used for the Formation of Strontium Titanate Bicrystals
Article Type:	Invited Methods Article - JoVE Produced Video
Keywords:	Grain boundary; bicrystal; electric field; spark plasma sintering
Manuscript Classifications:	92.27.10: crystal structure (nonmetallic materials); 92.27.11: crystals (nonmetallic); 92.27.14: evaluation of nonmetallic materials; 92.27.33: nonmetallic materials; 92.27.47: research on nonmetallic materials; 92.27.5: ceramic materials; 93.31: Engineering (General)
Corresponding Author:	Klaus van Benthem University of California Davis Davis, CA UNITED STATES
Corresponding Author Secondary Information:	
Corresponding Author E-Mail:	benthem@ucdavis.edu
Corresponding Author's Institution:	University of California Davis
Corresponding Author's Secondary Institution:	
First Author:	Lauren Hughes
First Author Secondary Information:	
Other Authors:	Lauren Hughes
Order of Authors Secondary Information:	
Abstract:	A spark plasma sintering apparatus was used as a novel method for diffusion bonding of two single crystals of strontium titanate to form bicrystals with one twist grain boundary. This apparatus utilizes high uniaxial pressure and a pulsed direct current for rapid consolidation of material. Diffusion bonding of strontium titanate bicrystals without fracture, in a spark plasma sintering apparatus, is possible at high pressures due to the unusual temperature dependent plasticity behavior of strontium titanate. We demonstrate a method for the successful formation of bicrystals at accelerated time scales and lower temperatures in a spark plasma sintering apparatus compared to bicrystals formed by conventional diffusion bonding parameters. Bond quality was verified by scanning electron microscopy. A clean and atomically abrupt interface containing no secondary phases was observed using transmission electron microscopy techniques. Local changes in bonding across the boundary was characterized by simultaneous scanning transmission electron microscopy and spatially resolved electron energy-loss spectroscopy.
Author Comments:	
Additional Information:	
Question	**Response**
If this article needs to be "in-press" by a certain date to satisfy grant requirements, please indicate the date below and explain in your cover letter.	

TITLE:
Spark Plasma Sintering Apparatus used for the Formation of Strontium Titanate Bicrystals

AUTHORS:
Hughes, Lauren A.
Materials Science and Engineering
University of California Davis
Davis, CA
lahughes@ucdavis.edu

van Benthem, Klaus
Materials Science and Engineering
University of California Davis
Davis, CA
benthem@ucdavis.edu

CORRESPONDING AUTHOR:
Klaus van Benthem
benthem@ucdavis.edu

Keywords:
Grain boundary; bicrystal; electric field; spark plasma sintering

SHORT ABSTRACT:
A viable technique for the formation of strontium titanate bicrystals at high pressure and fast heating rate via the spark plasma sintering apparatus is developed.

LONG ABSTRACT:
A spark plasma sintering apparatus was used as a novel method for diffusion bonding of two single crystals of strontium titanate to form bicrystals with one twist grain boundary. This apparatus utilizes high uniaxial pressure and a pulsed direct current for rapid consolidation of material. Diffusion bonding of strontium titanate bicrystals without fracture, in a spark plasma sintering apparatus, is possible at high pressures due to the unusual temperature dependent plasticity behavior of strontium titanate. We demonstrate a method for the successful formation of bicrystals at accelerated time scales and lower temperatures in a spark plasma sintering apparatus compared to bicrystals formed by conventional diffusion bonding parameters. Bond quality was verified by scanning electron microscopy. A clean and atomically abrupt interface containing no secondary phases was observed using transmission electron microscopy techniques. Local changes in bonding across the boundary was characterized by simultaneous scanning transmission electron microscopy and spatially resolved electron energy-loss spectroscopy.

INTRODCTION:
Spark plasma sintering (SPS) is a technique in which application of high uniaxial pressure and pulsed direct current leads to the rapid densification of powder compacts[1]. This technique also leads to the successful formation of composite structures from various materials, including

silicon nitride/silicon carbide, zirconium boride/silicon carbide, or silicon carbide, with no additional sintering aids required[2-5]. The synthesis of these composite structures by conventional hot-pressing had been challenging in the past. While application of a high uniaxial pressure and fast heating rate via the SPS technique enhances consolidation of powders and composites, the phenomenon causing this enhanced densification debated in the literature[2,3,6,7]. There also exists only limited information regarding the influence of electric fields on grain boundary formation and the resulting atomic structures of grain boundary cores[8,9]. These core structures determine the functional properties of SPS sintered materials, including electric breakdown of high voltage capacitors and the mechanical strength and toughness of ceramic oxides[10]. Therefore, understanding the fundamental grain boundary structure as a function of SPS processing parameters, such as applied current, is necessary for the manipulation of a material's overall physical properties. One method to systematically elucidate the fundamental physical mechanisms underpinning SPS is the formation of specific grain boundary structures, i.e., bicrystals. A bicrystal is created by manipulation of two single crystals, which are then diffusion bonded with specific misorientation angles [11]. This method provides a controlled way to investigate the fundamental grain boundary core structures as a function of processing parameters, dopant concentration, and impurity segregation[12-14].

Diffusion bonding is dependent on four parameters: temperature, time, pressure, and bonding atmosphere[15]. Conventional diffusion bonding of strontium titanate ($SrTiO_3$, STO) bicrystals typically occurs at a pressure below 1 MPa, within a temperature range of 1400-1500 °C, and time scales ranging from 3 to 20 hours[13,14,16,17]. In this study, bonding in a SPS apparatus is achieved at significantly lower temperature and time scales in comparison to conventional methods. For polycrystalline materials, reduced temperature and time scales via SPS significantly limits grain growth, thereby providing advantageous control of a material's properties through manipulation of its microstructure.

The SPS apparatus, for a 5×5 mm^2 sample, exerts a minimum pressure of 140 MPa. Within the conventional diffusion bonding temperature range, Hutt *et al.* report instantaneous fracture of STO when the bonding pressure exceeds 10 MPa[18]. However, STO exhibits temperature dependent plasticity behavior, indicating bonding pressure can exceed 10 MPa at specific temperatures. Above 1200 ˚C and below 700 ˚C, STO exhibits some ductility, at which stresses greater than 120 MPa can be applied without instantaneous fracture of the sample. Within the intermediate temperature range of 700-1200 ˚C, STO is brittle and experiences instantaneous fracture at stresses greater than 10MPa. At 800 ˚C, STO has minor deformability prior to fracture at stresses less than 200 MPa [19-21]. Hence, bonding temperatures for STO bicrystal formation via SPS apparatus must be selected according to the plasticity behavior of the material.

PROTOCOL:

1) Sample preparation of single crystal strontium titanate.

Note: Single crystal STO is supplied with a (100) surface polished to a mirror finish.

1.1) Section STO into 5x5 mm^2 pieces using diamond wire saw.

1.2) Ultrasonically clean samples at 50-60 Hz consecutively in baths of acetone, isopropanol, and methanol for fifteen minutes each.

1.3) Remove STO from methanol bath to immediately place on Bunsen burner held at a temperature of 200 ˚C. Heating the sample after cleaning prevents formation of evaporation spotting from the alcohol.

1.4) Place samples for ten minutes in buffered hydrofluoric acid (pH=4), a 6:1 solution of ammonium fluoride and 49% hydrofluoric acid.[22] This solution etches the STO, forming a predominantly (100) TiO_2 terminated surface. If the optically flat side of the single crystal has a rainbow patina, the sample has been over-etched and should not be used.

1.5) After ten minutes in the etchant solution, rinse samples in deionized (DI) water and then in isopropanol. Dry using clean house air.

2) Bicrystal formation via spark plasma sintering apparatus.

Note: For 5x5 mm^2 crystal use a 30 mm diameter graphite die. If a die with a diameter smaller than 30 mm is used, the bicrystal catastrophically fractures during bonding. Optimal die size as well as pressure exerted by the SPS apparatus is highly dependent on the size of the crystals.

2.1) Place a 30 mm circle of graphite paper on a graphite plunger with a 30 mm diameter. Graphite paper prevents STO from bonding to the graphite plunger during the experiment.

2.2) Stack two 5x5 mm^2 STO single crystals with their optically flat surfaces placed facing inward to form the bicrystal boundary. Center the stack on top of the graphite paper and plunger.

2.3) Rotate the top single crystal around the <100> axis to a chosen misorientation angle. The <100> axis is perpendicular to the optically flat surface of crystal.

2.4) Slide the graphite die over the plunger and crystals. Place a second 30 mm diameter circle of graphite paper and then 30 mm diameter plunger over the stacked STO crystals.

2.5) Stack the combined plungers and die onto the graphite spacers in SPS apparatus (Figure 1).

2.6) Apply a uniaxial force of 3 kN to minimize contact resistance using the z-axis control buttons. Throughout the experiment, keep the force at 3 kN via the z-axis control buttons.

2.7) Insert k-type thermocouple into graphite die at the small hole, shown in Figure 1. The thermocouple extends through the die to the sample.

2.8) Set the chamber pressure of the SPS apparatus to ~10 Pa using the vacuum push buttons.

2.9) Select bond temperature, time, and heating rates via program instrument control software (Table 1). For the bonding temperature and time, use a heating rate of 70-80 ˚C/minute and a cooling rate of 50 °C/minute.

2.10) Set 12 second on, 2 second off DC pulse using the instrument sintering button. A pulsed bias of ~ 4 V and direct current of ~550 A are applied incrementally to the sample once the program is set to run.

2.11) Press the start button on the machine.

2.12) Remove the sample when the program ends. After bicrystal formation, the sample will appear grey-black due to the reducing environment of the SPS apparatus.

2.13) Use a high temperature furnace at a temperature of 1200 ˚C for 140 hours, apply no pressure during this procedure, to anneal and re-oxidize the sample in air. Annealing parameters were selected according to previous work done by Hutt *et al* in which bicrystals formed in high vacuum[13]. After annealing, the sample reveals an off-white color and is oxidized.

3) Sample preparation of bicrystal for electron beam imaging.

3.1) Cross-section bicrystal with diamond wire saw into 5x1 mm^2 sections.

3.2) Polish cross-section samples with diamond lapping film. The grit size on the diamond lapping film is gradually decreased from 9 μm to 0.1 μm. Change to smaller grit size once scratches are uniform across the surface. Use a counter clockwise platen motion for 9 μm to 6 μm lapping film. Use a counter clockwise platen motion with an oscillating sample head for 6 μm to 0.1 μm lapping film.

3.3) Polish cross-section samples with colloidal silica for two minutes using a mat cloth. Continuously pour colloidal silica onto the mat with counter clockwise platen motion and oscillating sample head.

3.4) Fifteen seconds before removing the sample, stop pouring colloidal silica and pour DI water onto platen. Pour DI water for fifteen seconds, remove sample, and immediately rinse sample in DI water for 1 minute. If this procedure is not followed, the colloidal silica will bond the sample's surface and obscure the grain boundary during scanning electron microscopy (SEM).

3.5) Once the sample is polished to an optically smooth surface, ultrasonically clean samples consecutively in baths of acetone, isopropanol, and methanol for fifteen minutes each.

3.6) Remove STO from methanol bath to immediately place on Bunsen burner held at a temperature of 200 ˚C. Heating the sample after cleaning prevents formation of evaporation spotting from the alcohol.

3.7) Mount sample polished surface up onto a sample stub using colloidal graphite.

3.8) Sputter coat sample surface with 2-3 nm of carbon. Use the following parameters for the carbon coater: a pulse resolution of .2 nm/pulse, current step rate of .2 A/pulse, pulse current of 40 A, pulse length of 2 s, and maximum pulses of 50.

4) Cleaning the FIB copper grid.

Note: Improper cleaning of the FIB grid can lead to carbon contamination of the lamella in the TEM.

4.1) Place copper FIB grid in an acetone and then isopropanol bath for 1 h each.

4.2) Plasma clean copper FIB grid for 10 minutes.

5) Preparation of transmission electron microscopy (TEM) lamella via focused ion beam (FIB) apparatus.

Note: All parameters used in FIB preparation are typed or selected from a drop down menu in the FIB apparatus software.

5.1) Place STO sample and copper FIB grid in FIB apparatus. The stage is at 7 mm.

5.2) Find a region of interest along the interface between the two single crystals, i.e. the grain boundary.

5.3) Select Patterning dialogue box. In Patterning Control, select the Rectangle Patterning Tool with application property C-e-dep surface. Insert C-dep for gas injection. Deposit a 15×2×2 μm^3 protective layer of carbon using the electron beam at a voltage of 5.0 kV, a current of 13.0 nA, and a tilt angle of 0˚. Retract C-dep.

5.4) Select Patterning dialogue box. In Patterning Control, select the Rectangle Patterning Tool with application property W-dep. Insert W-dep for gas injection. Deposit 15×2×2 μm^3 protective layer of tungsten using the ion beam at a voltage of 30.0 kV, a current of 0.3 nA, and a tilt angle of 52˚. Retract W-dep.

5.5) Select Patterning dialogue box. In Patterning Control, select the Regular Cross Section Patterning Tool with application property Si. Use 22×25×15 μm^3 for the bottom pattern and of 22×27×15 μm^3 for the top pattern at a voltage of 30.0 kV, a current of 30.0 nA, and a tilt angle of 52˚ via the ion beam. The pattern will create a trench mill on both sides of the protective layer.

5.6) Select Patterning dialogue box. In Patterning Control, select the Clean Cross Section Patterning Tool with application property Si. Use 22×3×60 μm^3 for the top and bottom pattern at a voltage of 30.0 kV and a current of 1.0 nA via the ion beam. The tilt angle is 53.5˚ for the bottom pattern and 50.5˚ for the top pattern. The pattern cleans the surface of the trenched lamella from the curtaining pattern that results from the regular cross section patterning.

5.7) Cut a J-pattern into the sample using the Rectangle Patterning tool with application property Si. Use 2 µm for the width at a voltage of 30.0 kV and a current of 1.0 nA via the ion beam.

5.8) Select Easy Lift dialogue box. Insert the micromanipulator to the park position. Lower the micromanipulator and attach the sample to the copper FIB grid via a tungsten weld using the process detailed in 5.4.

5.9) Using the steps detailed in 5.7, cut a U-pattern, continuing from the original J-pattern, in the sample using the ion beam at a voltage of 30.0 kV and a current of 1.0 nA.

5.10) Lift the lamella via the micromanipulator above the bulk sample. Rotate the micromanipulator 180˚, so the grain boundary is no longer parallel to ion beam, but perpendicular to the ion beam.

5.11) Tungsten weld the lamella to a copper FIB grid using the steps detailed in 5.4 with the ion beam at a voltage of 30.0 kV and a current of 0.3 nA.

5.12) Cut the micromanipulator from the lamella using the steps detailed in 5.7 with the ion beam at a voltage of 30.0 kV and a current of 1.0 nA.

5.13) Repeat the steps detailed in 5.3. Deposit a 15×2×4 μm^3 protective layer of carbon using an electron beam at a voltage of 5.0 kV, a current of 13.0 nA, and a tilt angle of 0˚.

5.14) Repeat the steps detailed in 5.4. Deposit 15×2×8 μm^3 protective layer of tungsten using an ion beam at a voltage of 30.0 kV, a current of 0.3 nA, and a tilt angle of 52˚.

5.15) With the ion beam, thin the sample to approximately 200 nm using a voltage of 30.0 kV and a systematically decreasing current of 0.5 nA, 0.3 nA, and 0.1 nA. At this stage, a cleaning cross section pattern is used and the sample is tilted to an angle of 52 ± 1.5˚.

5.16) With the ion beam, thin the sample to electron transparency using a voltage of 5.0 kV and a current of 77.0 pA. At this stage, a rectangle pattern is used with a tilt angle of 52 ± 3˚.

5.17) Remove amorphous damage incurred from the FIB by cleaning the sample at a voltage of 500 eV and a current of 150 µA.

REPRESENTIVE RESULTS:

Bonding temperature, time, and misorientation angle were all altered to determine optimum parameters needed for the maximum possible bonded interface fraction of the STO bicrystal (Table 1). The interface was considered ‘bonded’ when the grain boundary was not visible during SEM imaging (Figure 2a). A ‘non-bonded’ interface was exhibited when a dark image contrast or voids were present at the boundary location (Figure 2b). Dark image contrast signified colloidal graphite from the FIB mounting procedure had diffused between the two STO crystals due to capillary effects. This non-bonded interface is observed at the edges of the bicrystal, while the bonded interface is observed at the center of the bicrystal. The change in bonding behavior from the edge to the center of the bicrystals formed by SPS apparatus is also seen in bicrystals formed via hot pressing techniques[6].

Micro-crack formation in the bulk of the bicrystal is observed in all samples. For successfully bonded bicrystals, micro-crack formation does not interfere with the bonded interface. At a bonding temperature of 1200 °C, extensive micro-cracking occurs, leading to brittle failure of the bicrystal during annealing. Therefore, bonding temperature in the SPS apparatus was kept below 800 ˚C to prevent catastrophic fracture.

For bicrystals with 0° misorientation angle at bonding temperatures of 600 ˚C and 700 ˚C, a 95% successfully bonded interface was obtained. An increase in the misorientation angle of the bicrystal to 44.4° requires a bonding temperature of 800 ˚C and bonding time of 90 minutes to achieve a 45.8% successfully bonded interface. High resolution TEM (HRTEM) and high angle annular dark field scanning transmission electron microscopy (HAADF-STEM) micrographs of this sample reveal an atomically abrupt grain boundary structure with no intergranular film or secondary phases present (Figure 3). Spatially resolved electron energy loss spectroscopy (EELS) recorded directly from the interface shows a reduction in the crystal field splitting of the Ti L_3 and L_2 edges as well as a reduction in the O K edge intensity when compared to the bulk (Figure 4).

Table 1. Bonding Parameters and Subsequent Interface Fraction of Bicrystals.
SPS apparatus diffusion bonding parameters and subsequent bonded interface fractions of STO bicrystals. A pulsed bias voltage of ~4 V and direct current of ~550 A is applied for all experiments. Bonded interface fractions were calculated from an average grain boundary length of (1.5±0.4) mm. These regions were taken from varying areas within the bicrystal.

Figure 1. Spark Plasma Sintering Apparatus.
Set up for the spark plasma sintering apparatus. Pressure is applied perpendicular to the bicrystal interface.

Figure 2. Typical Interfaces Found in SPS Apparatus Formed Bicrystals.
Nominal 45˚ twist bicrystal formed at a temperature of 800 ˚C for 90 minutes (a) SEM image of defined bonded' interface, the grain boundary location is inferred by the presence of a faceted void, and (b) SEM image of the defined 'non-bonded' interface. Spherical beads observed in images are residual silica from polishing.

Figure 3. High Resolution Imaging of Bicrystal Grain Boundary.
Boundary of nominal 45˚ twist bicrystal formed at a temperature of 800 ˚C for 90 minutes recorded in <100> zone axis with an edge-on orientation for the interface plane (a) HRTEM image (b) HRSTEM DF image, and (c) structure model composed of two single crystals, one in <100> and one in <110> zone axis orientation with a {001} interface plane. Deviations of the experimental imaging data from the projected structure model represent changes of the interface configuration compared to the ideal single-crystal atom positions.

Figure 4. Structure and Chemistry of Bicrystal Grain Boundary.
Near edge fine structure of (a) the Ti $L_{2,3}$ edge and (b) the O K edge taken at the boundary and the bulk of 45˚ twist bicrystal formed at a temperature of 800 ˚C for 90 minutes.

Figure 5. FIB Milling at Bicrystal Grain Boundary.

HRTEM images of FIB TEM lamella of (a) sample with grain boundary parallel to the ion beam and (b) sample with grain boundary perpendicular to the ion beam.

DISCUSSION:

The bonding temperature of 1200 °C was chosen to maximize diffusion as small changes in temperature can greatly impact the kinetics of all diffusion bonding mechanisms. A temperature of 1200 ˚C is outside the brittle-ductile transition temperature range of STO. However, the sample underwent brittle fracture at this temperature. The catastrophic failure of the STO bicrystal was not unexpected as STO has ~ 0.5% ductility at 1200 °C. Also, the sample was held at a pressure of 140 MPa throughout the heating process and STO transitions through its brittle stage during this heating process where it has 0% ductility[21]. Thus successful diffusion bonding of single crystals via the SPS apparatus necessitates an in-depth understanding of the temperature dependent plasticity behavior of a material.

Two bicrystals were formed using a bonding temperature of 800 ˚C and a bonding time of 20 minutes. The bicrystal with a nominal misorientation of 4˚ was annealed for 50 hours and exhibited a bonded interface fraction 2.2x greater than the bicrystal with nominal misorientation of 45˚, annealed for 140 hours. Annealing times longer than 50 hours did not reveal any significant improvement of the diffusion bonding quality. Annealing temperature and time were selected according to previous work in which the bicrystals were formed in a high vacuum furnace, similar to the SPS apparatus[11]. To ascertain if there was an impact of the annealing process on the diffusion bonding of these bicrystals, diffusion bond lengths were calculated and found to be 0.27 nm at a temperature of 1200 ˚C for 140 hrs[23]. The selected annealing parameters, therefore, only had limited impact on the diffusion bonding of the bicrystal. This analysis was further supported when the diffusion bonding of a bicrystal with a 45° twist misorientation was not successful for the same parameters utilized during annealing.

While the selected annealing parameters did not significantly impact the diffusion bonding, the misorientation angle does have a pronounced effect. High-angle misorientation angles create a greater structural mismatch between the two half-crystals, which hinders cross diffusion and decreases interface bonding. For high misorientation angles, bonding temperature and time must be increased in order to have a larger successfully bonded interface fraction.

Bicrystal formation via SPS processing techniques occurs at significantly accelerated times scales and moderate temperature ranges compared to the conventional hot press methods. This difference in processing parameters between conventional diffusion bonding and the SPS method is also seen in the formation of powder compacts and composites. As mentioned above, bicrystals formed via conventional diffusion bonding methods are formed at temperatures greater than 1400 ˚C with times scales ranging from 3 to 20 hours[11,24]. Using a SPS instrument, diffusion bonding occurs at a temperature of 800 ˚C with times scales ranging from 20 to 90 minutes. The SPS technique is then useful for the rapid diffusion bonding of bicrystals compared to conventional methods. Bicrystal formation by the SPS instrument also allows for experimental observation of the mass transfer mechanisms at a grain boundary with a selected misorientation. This experimental observation will provide more insight into the mechanisms underpinning the SPS technique.

Micro-cracks in the bulk STO bicrystal prevented conventional mechanical TEM lamella preparation. The mechanical thinning process led to fracture of the TEM lamella due to micro-cracks spreading throughout the bulk. Therefore, FIB preparation of the TEM lamella was used. Conventional FIB lift-out of the lamella, in which the grain boundary is parallel to the ion beam, led to preferential milling along the interface plane (Figure 5a). The FIB preparation technique was subsequently modified. First, the thickness of the initial protective layer of carbon and tungsten was selected so, at the end of the lift-out step, the protective layer was milled away. If the protective layer was too thick and remained throughout the thinning process, re-deposition of tungsten occurred and obscured TEM analysis. Secondly, after the TEM lamella was attached to the tip of the micromanipulator, the micromanipulator was rotated by 180˚. This rotation caused the grain boundary to become perpendicular to the ion beam, hence preventing preferential thinning (Figure 5b). Lastly, after the lift-out process, protective layers of carbon and tungsten were deposited onto the surface of the newly oriented TEM lamella. These modifications to the conventional FIB preparation technique led to a clean TEM lamella enabling atomically resolution imaging by HAADF-STEM.

HRTEM and HAADF-STEM micrographs for the bicrystal bonded at 800 ˚C for 90 minutes with a nominal 45˚ twist grain boundary show an atomically resolved grain boundary structure with no secondary phases. Spatially resolved EELS reveal changes in the Ti coordination within the grain boundary cores, indicating an increase in the oxygen vacancy concentration compared to the bulk. These results are consistent with reports in the literature for low-angle twist grain boundaries[25]. Further analysis of these experiments is described elsewhere[26].

In this study, STO bicrystals were successfully synthesized for the first time using a SPS apparatus. Bicrystals with twist orientations of 0˚, 4˚, and 45˚ were formed at high pressure with moderate bonding temperatures and time scales compared to those parameters found in conventional bonding. Formation of bicrystals via the SPS apparatus provides an opportunity to quantitatively determine the impact of electric field as well as heating rate on selected grain boundary core structures.

ACKNOWLEDGEMENTS:
LH gratefully acknowledges financial support by an US National Science Foundation Graduate Research Fellowship under Grant No. 1148897. Electron microscopy characterization and SPS processing at UC Davis was financially supported by a University of California Laboratory Fee award (#12-LR-238313). *Work at the Molecular Foundry was supported by the Office of Science, Office of Basic Energy Sciences, of the U.S. Department of Energy under Contract No. DE-AC02-05CH11231.*

DISCLOSURE:
We have nothing to disclose.

REFERENCES
1 Munir, Z. A., Anselmi-Tamburini, U. & Ohyanagi, M. The effect of electric field and pressure on the synthesis and consolidation of materials: A review of the spark plasma sintering method. *J. Mater. Sci.* **41** (3), 763-777, doi:10.1007/s10853-006-6555-2 (2006).

2 Chen, W., Anselmi-Tamburini, U., Garay, J. E., Groza, J. R. & Munir, Z. A. Fundamental investigations on the spark plasma sintering/synthesis process: I. Effect of dc pulsing on reactivity. *Mater. Sci. Eng. A.* **394** (1–2), 132-138, doi:10.1016/j.msea.2004.11.020 (2005).
3 Holland, T. B., Anselmi-Tamburini, U. & Mukherjee, A. K. Electric fields and the future of scalability in spark plasma sintering. *Scr. Mater.* **69** (2), 117-121, doi:10.1016/j.scriptamat.2013.02.047 (2013).
4 Wan, J., Duan, R. & Mukherjee, A. Spark plasma sintering of silicon nitride/silicon carbide nanocomposites with reduced additive amounts. *Scr. Mater.* **53** (6), 663-667, doi:10.1016/j.scriptamat.2005.05.037 (2005).
5 Carney, C. M., Mogilvesky, P. & Parthasarathy, T. A. Oxidation Behavior of Zirconium Diboride Silicon Carbide Produced by the Spark Plasma Sintering Method. *J. Amer. Ceram. Soc.* **92** (9), 2046-2052, doi:10.1111/j.1551-2916.2009.03134.x (2009).
6 Dupeux, M. Production of Oriented Two-Phase Bicrystals by Diffusion Bonding Technique. *J. Cryst. Growth.* **66** 169-178 (1984).
7 Castro, R. & van Benthem, K. *Sintering: mechanisms of convention nanodensification and field assisted processes*. Vol. 35 (Springer Science & Business Media, 2012).
8 Byeon, S. C. & Hong, K. S. Electric field assisted bonding of ceramics. *Mater. Sci. Eng. A.* **287** (2), 159-170 (2000).
9 Wang, J. & Conrad, H. Contribution of the space charge to the grain boundary energy in yttria-stabilized zirconia. *J. Mater. Sci.* **49** (17), 6074-6080, doi:10.1007/s10853-014-8331-z (2014).
10 Fujimoto, M. & Kingery, W. D. Microstructures of SrTiO3 Internal Boundry Layer Capacitors During and After Processing and Resultant Electrical Properties. *J. Amer. Ceram. Soc.* **68** (4), 169-173 (1985).
11 Mitsuma, T. *et al.* Structures of a Σ = 9, [110]/{221} symmetrical tilt grain boundary in SrTiO3. *J Mater Sci.* **46** (12), 4162-4168, doi:10.1007/s10853-011-5266-5 (2011).
12 Ikuhara, Y. Grain Boundary and Interface Structures in Ceramics. *J. Ceram. Soc. Jpn.* **109** (7), S110-S120 (2001).
13 Hutt, S., Kienzle, O., Ernst, F. & Ruhle, M. Processing and Structure of Grain boundaries in Strontium Titanate. *Z. Metallkd.* **92** (2), 105-109 (2001).
14 Takahisa, Y., Ikuhara, Y. & Sakuma, T. Current-voltage characteristics across 45◦ symmetric tilt boundary in highly donor-doped SrTiO3 bicrystal. *J. Mater. Sci. Lett.* **20** 1827-1829 (2001).
15 Hill, A. & Wallach, E. R. Modelling Solid State Diffusion Bonding. *Acta Metall.* **37** (9), 2425-2437 (1989).
16 Sato, Y. *et al.* Non-linear current–voltage characteristics related to native defects in SrTiO3 and ZnO bicrystals. *Sci. Technol. Adv. Mater.* **4** (6), 605-611, doi:10.1016/j.stam.2003.10.031 (2003).
17 Hirose, S., Nishimura, H. & Niimi, H. Resistance switching effect in Nb-doped SrTiO[sub 3] (100) bicrystal with (100) ∼45° twist boundary. *J. App. Phys.* **106** (4), 043714-043711-043716, doi:10.1063/1.3204476 (2009).
18 Hutt, S. Doctoral Thesis. *University of Stuttgart.* (2002).
19 Brunner, D., Taeri-Baghbadrani, S., Sigle, W. & Ruhle, M. Suprising Results of a Studay on the Plasticity in Strontium Titanate. *J. Amer. Ceram. Soc.* **84** (5), 1161-1163 (2001).

20 Gumbsch, P., Taeri-Baghbadrani, S., Brunner, D., Sigle, W. & Ruhle, M. Plasticity and an inverse brittle-to-ductile transition in strontium titanate. *Phys. Rev. Lett.* **87** (8), 085505-085501-085504, doi:10.1103/PhysRevLett.87.085505 (2001).
21 Taeri, S., Brunner, D., Sigle, W. & Ruhle, M. Deformation Behavior of Strontium Titanate between Room Temperature and 1800K under Ambient Pressure. *Z. Metallkd.* **95** 433-446 (2004).
22 Takahashi, K., Ohtomo, A., Kawasaki, M. & Koinuma, H. Advanced Processing and Characterization of SrTiO3 Single Crystals and Bicrystals for High Tc Superconducting Film Substrate. *Mater. Sci. Eng. B.* **B41** 152-156 (1996).
23 Rhodes, W. H. & Kingery, W. D. Dislocation Dependence of Cationic Diffusion in SrTiO3. *J. Amer. Ceram. Soc.* **49** (10), 521-526 (1966).
24 Yamamoto, T., Hayashi, K., Ikuhara, Y. & Sakuma, T. Grain Boundary Structure and Electrical Properties in Nb-Doped SrTiO₃ Bicrystals. *Key Eng. Mater.* **181-182** 225-230, doi:10.4028/www.scientific.net/KEM.181-182.225 (2000).
25 Fitting, L., Thiel, S., Schmehl, A., Mannhart, J. & Muller, D. A. Subtleties in ADF imaging and spatially resolved EELS: A case study of low-angle twist boundaries in SrTiO3. *Ultramicroscopy.* **106** (11-12), 1053-1061, doi:10.1016/j.ultramic.2006.04.019 (2006).
26 Hughes, L. A. & van Benthem, K. Formation of SrTiO3 bicrystals using spark plasma sintering techniques. *Scr. Mater.* **118** 9-12, doi:10.1016/j.scriptamat.2016.03.005 (2016).

Figure 1

Click here to download Figure Jove_Figure 1 SPS.pdf

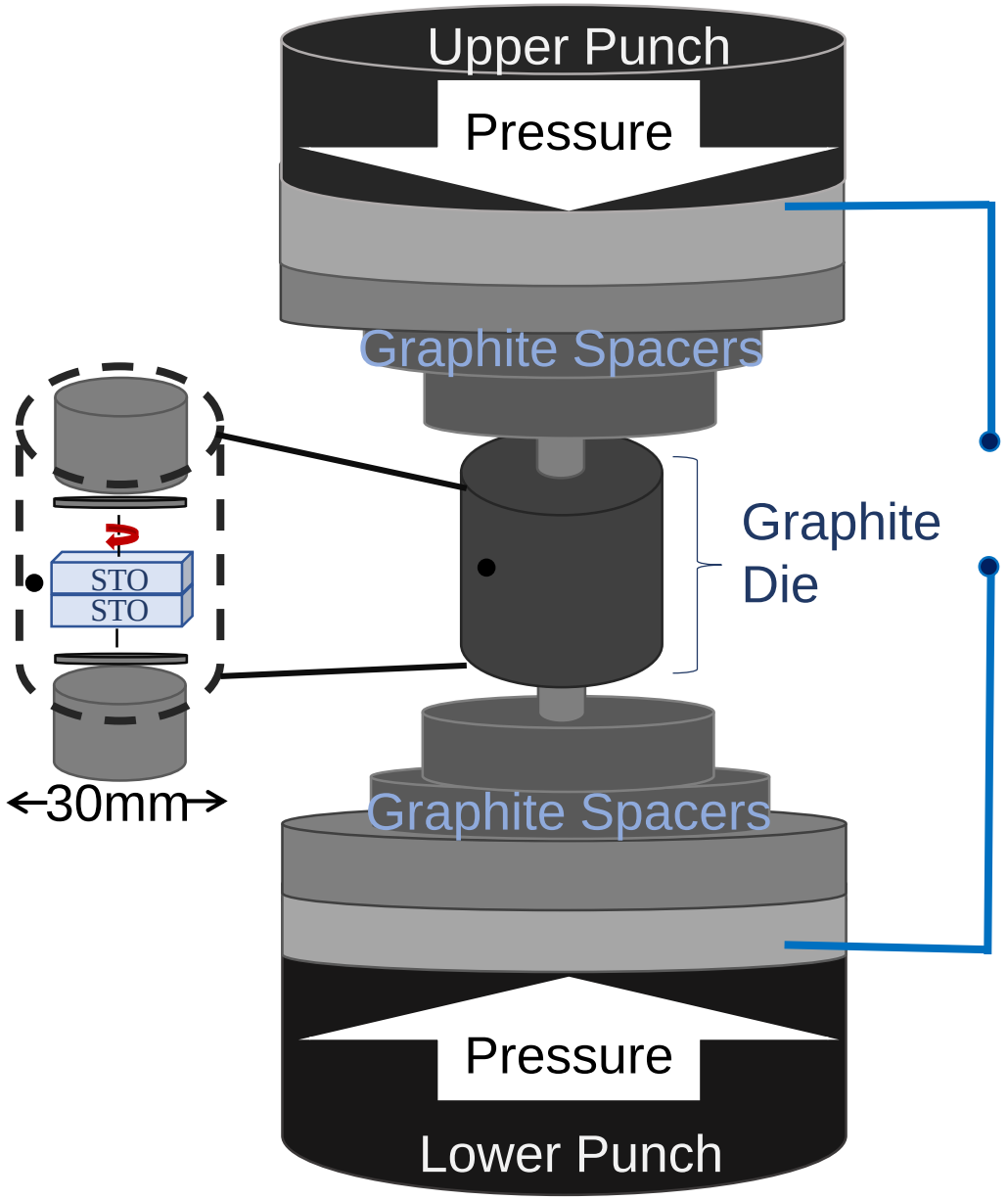

Figure 2

Click here to download Figure Jove_Figure 2 SEM.pdf

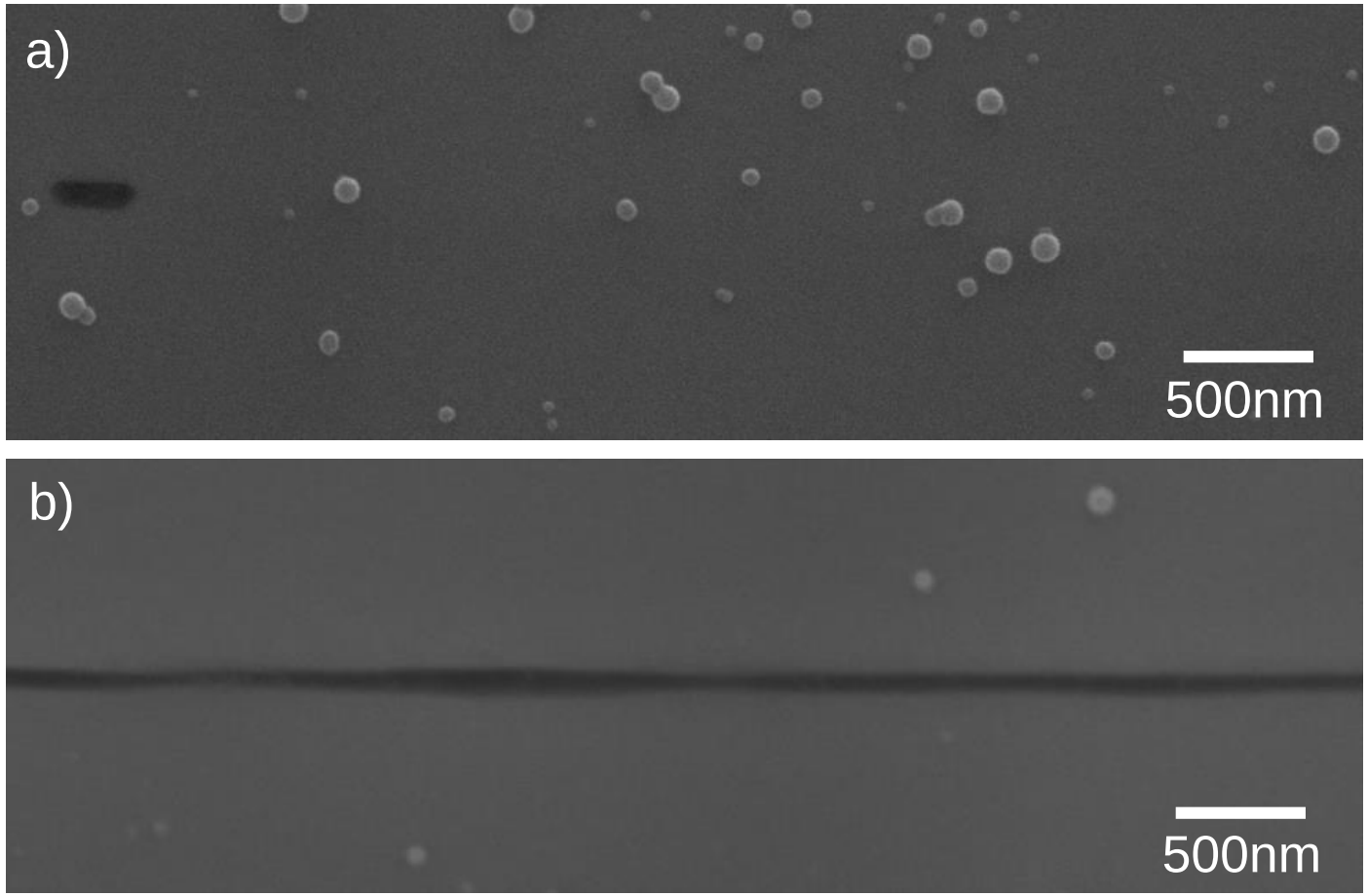

Figure 3

Click here to download Figure Jove_Figure 3_HAADFSTEM_2.pdf

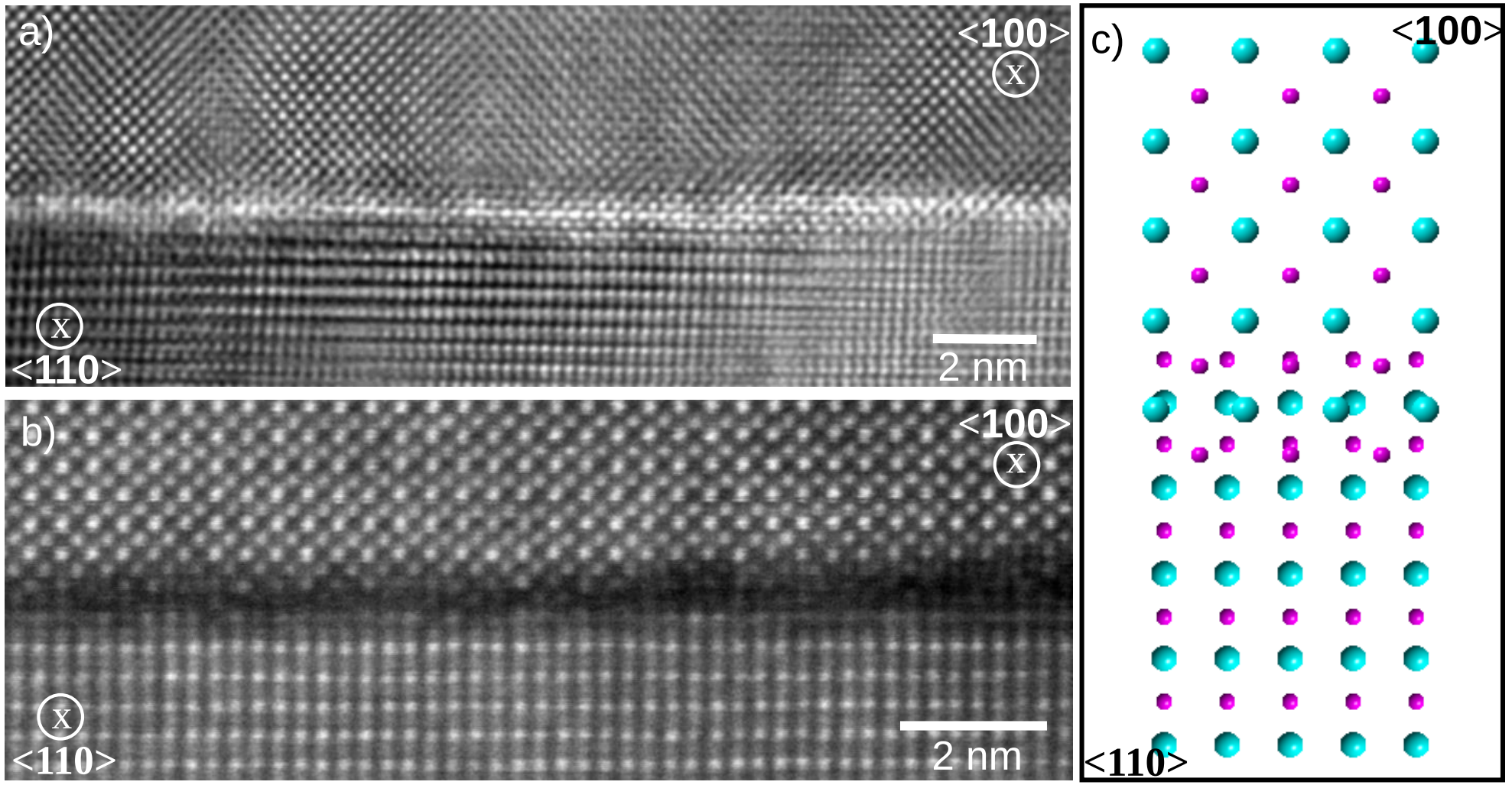

Figure 4

Click here to download Figure Jove_Figure 4_EELS.pdf

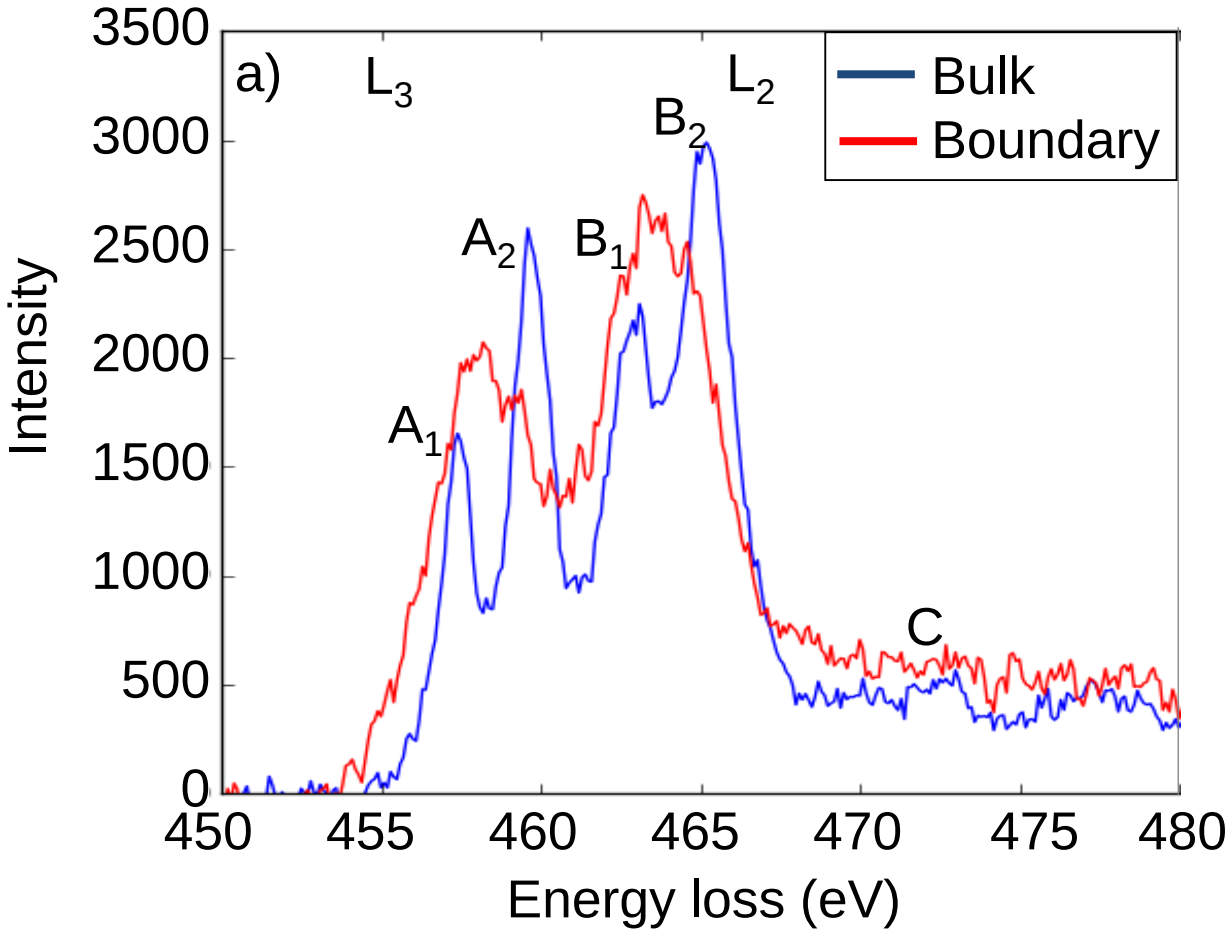

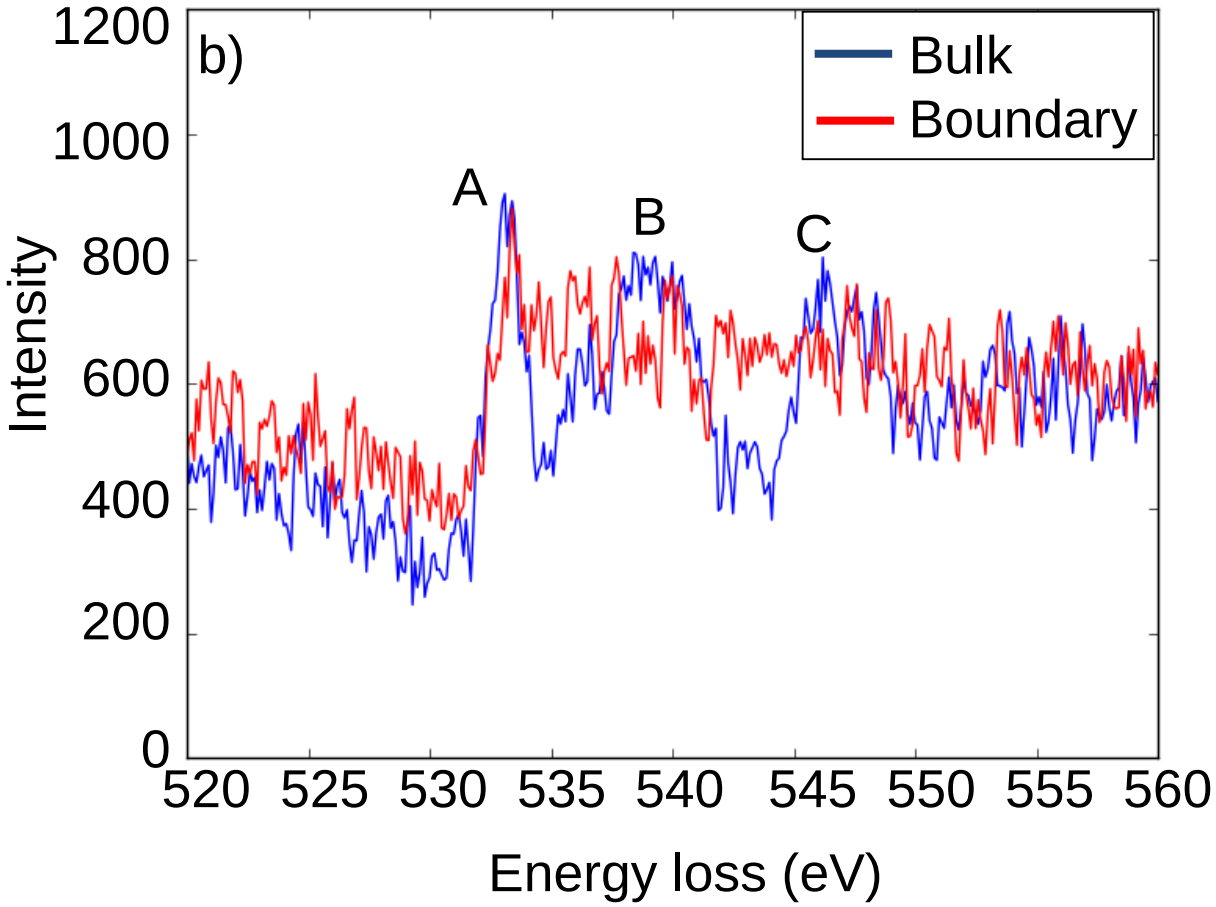

Figure 5

Click here to download Figure Jove_Figure 5_FIB.pdf

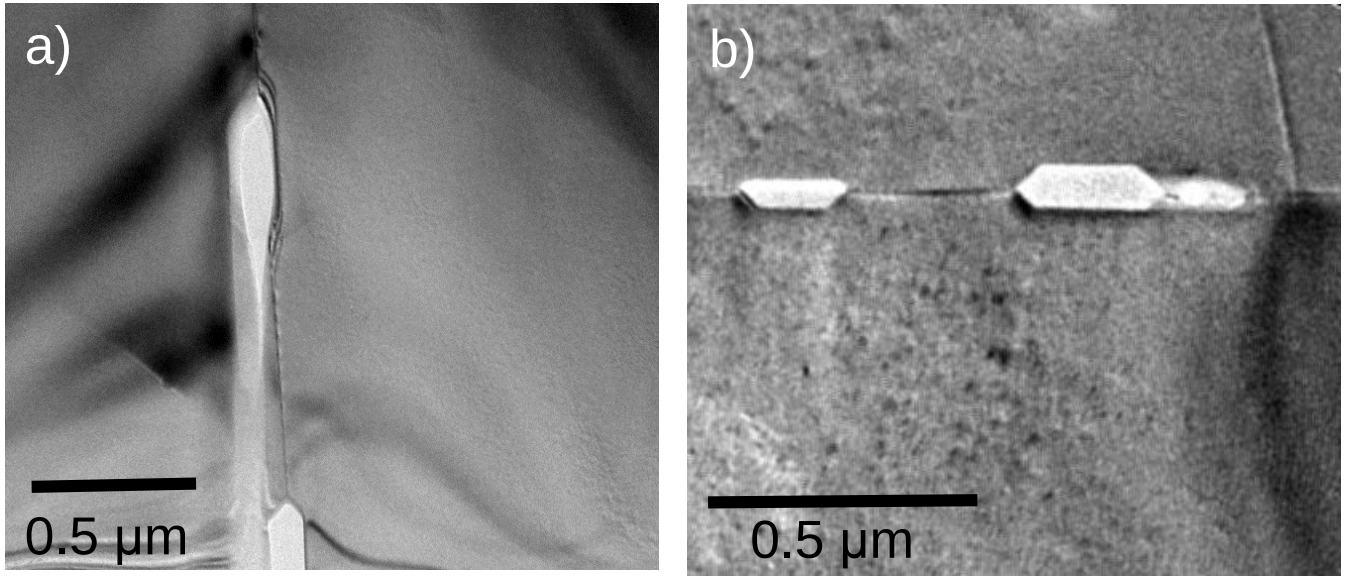

Bicrystal	Twist Orientatio	Bond Temperature	Bond Time (min)
A	0*	1200	15
B	0	600	90
C	0	700	90
D	4.3 ± .3	800	20
E	45*	700	60
F	46.1± .5	800	20
G	44.4± .1	800	90

Anneal Temperature (˚C)	Anneal Time (h)
1200	16
1200	100
1200	100
1200	50
1200	140
1200	140
1200	140

Bonded Interface ± .3 (%)
--
92.3
99.7
79.2
1.3
35.4
45.8

Name of Material/ Equipment	Company
Strontium titanate single crystal (100)	MTI Corporation
Buffered oxide etch, hyrofluoric acid 6:1	JT Baker
Scanning electron microscope (SEM)	FEI
SPS apparatus	Sumitomo Coal Mining Co
High Temperature Furnace	Thermolyne
Ultrasonic Cleaner	Bransonic
Mechanical polisher	Allied High Tech Products
Diamond lapping film	3M
Diamond lapping film	3M
Colloidal silica	Allied High Tech Products
Sputter coater	QuorumTech
Focused ion beam (FIB) instrument	FEI
Nanomill TEM specimen preparation system	Fischione Instruments
Transmission electron microscope (TEM)	JEOL
Scanning transmission electron microscope (STEM)	FEI

Catalog Number

STOa101005S1-JP
MBI 1178-03
Model: 430 NanoSEM
Model: Dr. Sinter 5000 SPS Apparatus
Model: 41600
Model: 221
15-2100-TEM
660XV
661X
180-20000
Model: Q150RES
Model: Scios dual-beamed focused ion beam (FIB) instrument
Model: 1040
Model: JEM2500 SE
Model: TEAM 0.5

Comments/Description

1 um to 9 um Grit Size
0.5 um to 0.1 um Grit Size
.05 um Grit Size

jove
1 Alewife Center 4000
Cambridge, MA 02140
tel. 617.945.9051
www.jove.com

ARTICLE AND VIDEO LICENSE AGREEMENT

Title of Article: Spark Plasma Sintering Apparatus used for the Formation of Strontium Titanate Bicrystals

Author(s): Lauren Hughes, Klaus van Benmem

Item 1 (check one box): The Author elects to have the Materials be made available (as described at http://www.jove.com/publish) via: ☑ Standard Access ☐ Open Access

Item 2 (check one box):

☒ The Author is NOT a United States government employee.

☐ The Author is a United States government employee and the Materials were prepared in the course of his or her duties as a United States government employee.

☐ The Author is a United States government employee but the Materials were NOT prepared in the course of his or her duties as a United States government employee.

ARTICLE AND VIDEO LICENSE AGREEMENT

1. Defined Terms. As used in this Article and Video License Agreement, the following terms shall have the following meanings: "**Agreement**" means this Article and Video License Agreement; "**Article**" means the article specified on the last page of this Agreement, including any associated materials such as texts, figures, tables, artwork, abstracts, or summaries contained therein; "**Author**" means the author who is a signatory to this Agreement; "**Collective Work**" means a work, such as a periodical issue, anthology or encyclopedia, in which the Materials in their entirety in unmodified form, along with a number of other contributions, constituting separate and independent works in themselves, are assembled into a collective whole; "**CRC License**" means the Creative Commons Attribution-Non Commercial-No Derivs 3.0 Unported Agreement, the terms and conditions of which can be found at: http://creativecommons.org/licenses/by-nc-nd/3.0/legalcode; "**Derivative Work**" means a work based upon the Materials or upon the Materials and other pre-existing works, such as a translation, musical arrangement, dramatization, fictionalization, motion picture version, sound recording, art reproduction, abridgment, condensation, or any other form in which the Materials may be recast, transformed, or adapted; "**Institution**" means the institution, listed on the last page of this Agreement, by which the Author was employed at the time of the creation of the Materials; "**JoVE**" means Myjove Corporation, a Massachusetts corporation and the publisher of *The Journal of Visualized Experiments*; "**Materials**" means the Article and / or the Video; "**Parties**" means the Author and JoVE; "**Video**" means any video(s) made by the Author, alone or in conjunction with any other parties, or by JoVE or its affiliates or agents, individually or in collaboration with the Author or any other parties, incorporating all or any portion of the Article, and in which the Author may or may not appear.

2. Background. The Author, who is the author of the Article, in order to ensure the dissemination and protection of the Article, desires to have the JoVE publish the Article and create and transmit videos based on the Article. In furtherance of such goals, the Parties desire to memorialize in this Agreement the respective rights of each Party in and to the Article and the Video.

3. Grant of Rights in Article. In consideration of JoVE agreeing to publish the Article, the Author hereby grants to JoVE, subject to **Sections 4** and **7** below, the exclusive, royalty-free, perpetual (for the full term of copyright in the Article, including any extensions thereto) license (a) to publish, reproduce, distribute, display and store the Article in all forms, formats and media whether now known or hereafter developed (including without limitation in print, digital and electronic form) throughout the world, (b) to translate the Article into other languages, create adaptations, summaries or extracts of the Article or other Derivative Works (including, without limitation, the Video) or Collective Works based on all or any portion of the Article and exercise all of the rights set forth in (a) above in such translations, adaptations, summaries, extracts, Derivative Works or Collective Works and (c) to license others to do any or all of the above. The foregoing rights may be exercised in all media and formats, whether now known or hereafter devised, and include the right to make such modifications as are technically necessary to exercise the rights in other media and formats. If the "Open Access" box has been checked in **Item 1** above, JoVE and the Author hereby grant to the public all such rights in the Article as provided in, but subject to all limitations and requirements set forth in, the CRC License.

jove
1 Alewife Center #200
Cambridge, MA 02140
tel. 617.945.9051
www.jove.com

ARTICLE AND VIDEO LICENSE AGREEMENT

4. Retention of Rights in Article. Notwithstanding the exclusive license granted to JoVE in **Section 3** above, the Author shall, with respect to the Article, retain the non-exclusive right to use all or part of the Article for the non-commercial purpose of giving lectures, presentations or teaching classes, and to post a copy of the Article on the Institution's website or the Author's personal website, in each case provided that a link to the Article on the JoVE website is provided and notice of JoVE's copyright in the Article is included. All non-copyright intellectual property rights in and to the Article, such as patent rights, shall remain with the Author.

5. Grant of Rights in Video – Standard Access. This **Section 5** applies if the "Standard Access" box has been checked in **Item 1** above or if no box has been checked in **Item 1** above. In consideration of JoVE agreeing to produce, display or otherwise assist with the Video, the Author hereby acknowledges and agrees that, Subject to **Section 7** below, JoVE is and shall be the sole and exclusive owner of all rights of any nature, including, without limitation, all copyrights, in and to the Video. To the extent that, by law, the Author is deemed, now or at any time in the future, to have any rights of any nature in or to the Video, the Author hereby disclaims all such rights and transfers all such rights to JoVE.

6. Grant of Rights in Video – Open Access. This **Section 6** applies only if the "Open Access" box has been checked in **Item 1** above. In consideration of JoVE agreeing to produce, display or otherwise assist with the Video, the Author hereby grants to JoVE, subject to **Section 7** below, the exclusive, royalty-free, perpetual (for the full term of copyright in the Article, including any extensions thereto) license (a) to publish, reproduce, distribute, display and store the Video in all forms, formats and media whether now known or hereafter developed (including without limitation in print, digital and electronic form) throughout the world, (b) to translate the Video into other languages, create adaptations, summaries or extracts of the Video or other Derivative Works or Collective Works based on all or any portion of the Video and exercise all of the rights set forth in (a) above in such translations, adaptations, summaries, extracts, Derivative Works or Collective Works and (c) to license others to do any or all of the above. The foregoing rights may be exercised in all media and formats, whether now known or hereafter devised, and include the right to make such modifications as are technically necessary to exercise the rights in other media and formats. For any Video to which this Section 6 is applicable, JoVE and the Author hereby grant to the public all such rights in the Video as provided in, but subject to all limitations and requirements set forth in, the CRC License.

7. Government Employees. If the Author is a United States government employee and the Article was prepared in the course of his or her duties as a United States government employee, as indicated in **Item 2** above, and any of the licenses or grants granted by the Author hereunder exceed the scope of the 17 U.S.C. 403, then the rights granted hereunder shall be limited to the maximum rights permitted under such statute. In such case, all provisions contained herein that are not in conflict with such statute shall remain in full force and effect, and all provisions contained herein that do so conflict shall be deemed to be amended so as to provide to JoVE the maximum rights permissible within such statute.

8. Likeness, Privacy, Personality. The Author hereby grants JoVE the right to use the Author's name, voice, likeness, picture, photograph, image, biography and performance in any way, commercial or otherwise, in connection with the Materials and the sale, promotion and distribution thereof. The Author hereby waives any and all rights he or she may have, relating to his or her appearance in the Video or otherwise relating to the Materials, under all applicable privacy, likeness, personality or similar laws.

9. Author Warranties. The Author represents and warrants that the Article is original, that it has not been published, that the copyright interest is owned by the Author (or, if more than one author is listed at the beginning of this Agreement, by such authors collectively) and has not been assigned, licensed, or otherwise transferred to any other party. The Author represents and warrants that the author(s) listed at the top of this Agreement are the only authors of the Materials. If more than one author is listed at the top of this Agreement and if any such author has not entered into a separate Article and Video License Agreement with JoVE relating to the Materials, the Author represents and warrants that the Author has been authorized by each of the other such authors to execute this Agreement on his or her behalf and to bind him or her with respect to the terms of this Agreement as if each of them had been a party hereto as an Author. The Author warrants that the use, reproduction, distribution, public or private performance or display, and/or modification of all or any portion of the Materials does not and will not violate, infringe and/or misappropriate the patent, trademark, intellectual property or other rights of any third party. The Author represents and warrants that it has and will continue to comply with all government, institutional and other regulations, including, without limitation all institutional, laboratory, hospital, ethical, human and animal treatment, privacy, and all other rules, regulations, laws, procedures or guidelines, applicable to the Materials, and that all research involving human and animal subjects has been approved by the Author's relevant institutional review board.

10. JoVE Discretion. If the Author requests the assistance of JoVE in producing the Video in the Author's facility, the Author shall ensure that the presence of JoVE employees, agents or independent contractors is in accordance with the relevant regulations of the Author's institution. If more than one author is listed at the beginning of this Agreement, JoVE may, in its sole discretion, elect not take any action with respect to the Article until such time as it has received complete, executed Article and Video License Agreements from each such author. JoVE reserves the right, in its absolute and sole discretion and without giving any reason therefore, to accept or decline any work submitted to JoVE. JoVE and its employees, agents and independent contractors shall have

jove
1 Alewife Center #200
Cambridge, MA 02140
tel. 617.945.9051
www.jove.com

ARTICLE AND VIDEO LICENSE AGREEMENT

full, unfettered access to the facilities of the Author or of the Author's institution as necessary to make the Video, whether actually published or not. JoVE has sole discretion as to the method of making and publishing the Materials, including, without limitation, to all decisions regarding editing, lighting, filming, timing of publication, if any, length, quality, content and the like.

11. Indemnification. The Author agrees to indemnify JoVE and/or its successors and assigns from and against any and all claims, costs, and expenses, including attorney's fees, arising out of any breach of any warranty or other representations contained herein. The Author further agrees to indemnify and hold harmless JoVE from and against any and all claims, costs, and expenses, including attorney's fees, resulting from the breach by the Author of any representation or warranty contained herein or from allegations or instances of violation of intellectual property rights, damage to the Author's or the Author's institution's facilities, fraud, libel, defamation, research, equipment, experiments, property damage, personal injury, violations of institutional, laboratory, hospital, ethical, human and animal treatment, privacy or other rules, regulations, laws, procedures or guidelines, liabilities and other losses or damages related in any way to the submission of work to JoVE, making of videos by JoVE, or publication in JoVE or elsewhere by JoVE. The Author shall be responsible for, and shall hold JoVE harmless from, damages caused by lack of sterilization, lack of cleanliness or by contamination due to the making of a video by JoVE its employees, agents or independent contractors. All sterilization, cleanliness or decontamination procedures shall be solely the responsibility of the Author and shall be undertaken at the Author's expense. All indemnifications provided herein shall include JoVE's attorney's fees and costs related to said losses or damages. Such indemnification and holding harmless shall include such losses or damages incurred by, or in connection with, acts or omissions of JoVE, its employees, agents or independent contractors.

12. Fees. To cover the cost incurred for publication, JoVE must receive payment before production and publication the Materials. Payment is due in 21 days of invoice. Should the Materials not be published due to an editorial or production decision, these funds will be returned to the Author. Withdrawal by the Author of any submitted Materials after final peer review approval will result in a US$1,200 fee to cover pre-production expenses incurred by JoVE. If payment is not received by the completion of filming, production and publication of the Materials will be suspended until payment is received.

13. Transfer, Governing Law. This Agreement may be assigned by JoVE and shall inure to the benefits of any of JoVE's successors and assignees. This Agreement shall be governed and construed by the internal laws of the Commonwealth of Massachusetts without giving effect to any conflict of law provision thereunder. This Agreement may be executed in counterparts, each of which shall be deemed an original, but all of which together shall be deemed to me one and the same agreement. A signed copy of this Agreement delivered by facsimile, e-mail or other means of electronic transmission shall be deemed to have the same legal effect as delivery of an original signed copy of this Agreement.

A signed copy of this document must be sent with all new submissions. Only one Agreement required per submission.

CORRESPONDING AUTHOR:

Name:	Klaus van Benthem
Department:	Materials Science
Institution:	University of California Davis
Article Title:	Spark Plasma Sintering Apparatus used for Formation of Strontium Titanate Bicrystals
Signature:	[signature] Date: 7/11/16

Please submit a signed and dated copy of this license by one of the following three methods:

1) Upload a scanned copy of the document as a pfd on the JoVE submission site;
2) Fax the document to +1.866.381.2236;
3) Mail the document to JoVE / Attn: JoVE Editorial / 1 Alewife Center #200 / Cambridge, MA 02139

For questions, please email submissions@jove.com or call +1.617.945.9051

REBUTTAL LETTER

Spark Plasma Sintering Apparatus used for the Formation of Strontium Titanate Bicrystals

Lauren A. Hughes & Klaus van Benthem

We thank the reviewers for their detailed and constructive comments. In the following, we address each comment in the necessary detail and outline the revisions applied to the originally submitted manuscript.

Editorial Comments

All editorial changes were applied as requested. Additions to the discussion were made to address the significance of the experimental work with respect to alternative methods. These additions can be found on page 8 of the revised manuscript and are outlined using MS-Word Track Corrections.

Reviewer #1:

1. Introduction. Some of the literature of Joining using SPS should be included. For example some interesting results were reported in the case of SiC and C/SiC composites.
We appreciate the comment by the referee and agree that specific mentioning of SPS as a joining technique will strengthen the manuscript. We have added the following text to the introduction of the revised manuscript on pages 1-2:

"This technique also leads to the successful formation of composite structures from various materials, including silicon nitride/silicon carbide, zirconium boride/silicon carbide, or silicon carbide, while no additional sintering aids are required.[2-5] The synthesis of such composite structures had been challenging in the past by using conventional hot-pressing. While application of a high uniaxial pressure and fast heating rates via the SPS technique enhances consolidation of powders and composites, the phenomenon causing this enhanced densification debated in the literature."

2. In the experimental micron is written as um instead of µm.
We have fixed these typos in the revised version of the manuscript.

3. It is not clear how the temperature was probed. Modelling and experimental work (Grasso et al.) suggest significant gradients developed in the punch/die/sample assembly.
We appreciate this important comment by the referee. In this study, the temperature was probed using a k-type thermocouple that was inserted into the graphite die and is in contact with the sample. We have clarified this aspect of the experimental setup in section 2.8 of the experimental procedure.

The referee is correct that previous studies (including Grasso et al.) have indeed observed temperature gradients within SPS samples. Consistent with these studies, a difference in bonding

behavior from the edge of the bicrystal, which exhibits non-bonding, to the center of the bicrystal, which exhibits successful bonding, was observed in our SPS experiments. Also, similar to the experiments reported here, changes in bonding behavior from the edge to the center of a sample were previously observed during bicrystal formation using hot pressing techniques (M. Dupeux, *Journal of Crystal Growth*, 66 (1984) 169-178.). We have clarified this aspect in the first paragraph of the results section.

4. In table 1 the average and peaks currant and voltages should be given. In figure 1, is there any current flowing across the sample? Are the sample electrochemically reduced during the process affection their conductivity? Is there any color change of the sample induced by the processing?

For all experiments, a pulsed bias of 4 V and direct current of 550 A were applied to the sample with a 12-2 second pulse sequence. This detail was added to section 2.11 of the experimental procedure as well as in the caption of Table 1.

We have indeed observed a processing induced color change of the sample as considered by the referee. When the STO bicrystal sample is removed from the SPS instrument, it shows grey-black color. After the post-annealing process, STO returns to its off-white color. This color change indicates, as expected, STO reduces during processing, and re-oxidizes due to post annealing (see also reference 11 of the revised manuscript). We have added appropriate language to sections 2.13 and 2.14 of the revised manuscript.

The referee's question whether any current flows through the sample is critical, though a definite answer can not be provided at this stage. During the reported experiments, current is most likely *not* flowing across the sample as undoped STO is considered a dielectric material with a dielectric breakdown strength of 8e(6) V/m. The voltage output for the SPS apparatus is 4 V with a field strength of approximately 4e(3) V/m for the sample size. While STO is reduced during the SPS process at an oxygen partial pressure of 2e(-6) atm and a temperature of 800˚C, the conductivity of STO is roughly 1e(-4) to 1e(-5) ohm-cm^{-1} (Balachandran, U., and N. G. Eror. *Journal of Solid State Chemistry* 39.3 (1981): 351-359.). Conductivity of graphite used in SPS instruments is 1e(3) ohm-cm^{-1} (Mersen, High Strength Graphite for Sintering). We, therefore, conclude current is most likely flowing through the graphite die rather than the STO sample.

5. It might be useful to add (as inset) a simulated atomic structure to replicate the atomic distribution seen in figure 3.

We thank the referee for this suggestions, and have added a model atomic structure to Figure 3. This structure model is composed of two single crystals, one in <100> and one in <110> zone axis orientation with a {001} interface plane. Deviations of the experimental imaging data from the projected structure model represent changes of the interface configuration compared to the ideal single-crystal atom positions. A more refined minimum energy structure model would need to be modeled from first principles and is beyond the scope of this publication. Appropriate language was added to the caption of Figure 3.

6. Is any oxygen reduction appreciated comparing before and after SPS using the techniques described in the paper (see figure 4)?

As discussed for point 4 above STO is reduced during SPS processing, and re-oxidized before subsequent TEM characterization. All EELS experiments were carried out on re-oxidized samples so any observed reduction close or within the grain boundary cores is an intrinsic property of the grain boundary rather than the processing conditions.

7. In the some of the figures the direction of the applied load should be given.
We thank the referee for this comment, which is addressed in Figure 1. The application of load is perpendicular to the grain boundary of the STO bicrystal.

8. To support the field currents effect, polarity induced effect should be seen. Is there any field/current effect seen resulting in asymmetric atomic distribution/microstructures?
We thank the referee for this intriguing comment. In fact, an asymmetric atomic structure should be expected around the grain boundary plane. The focus of this publication, however, is to demonstrate the optimal conditions for creating STO bicrystals with the SPS apparatus. A detailed atomic structure analysis is beyond the scope of this current paper, and requires sub-Ångström spatial resolution imaging conditions coupled with density functional theory. Asymmetry of the atomic structure across a grain boundary is more reliably ascertained from segregation profiles of dopant elements. Such experiments are currently underway.

Reviewer #2
1. Why did the authors perform post long-time annealing at 1200C after spark plasma sintering? According to Takehara et al. (J Mater Sci (2014) 49, 3962), SrTiO3 bicrystal can be formed at 1000 degree for 80 h. It is not clear whether the bicrystals were mainly bonded during the SPS process or post annealing process.
Annealing parameters were selected according to work done by Hutt *et al* (*Zeitschrift fur Metallkunde.* **92** (2), 105-109 (2001)), in which the bicrystals are formed at high vacuum. Annealing parameters in other studies, including Takehara et al., are selected for bicrystals formed in an ambient environment. To ascertain the impact of the post-annealing process on the diffusion bonding in this work, diffusion bond lengths were calculated and found to be 0.27 nm.It is therefore concluded that the post-annealing had limited impact on the diffusion bonding of the bicrystal created in this study. A control experiment for bicrystal bonding with a 45° twist misorientation did not result in sufficient interfacial bonding when carried out using only the post-annealing parameters. An appropriate discussion of the post-annealing and its effect on the diffusion bonding was added to the reviswed manusctipy in section 2.14 of the experimental procedure, and on page 8 within the discussion section.

2. Is any pressure applied during the post annealing processes?
No pressure was applied during the post-annealing process. We have clarified the language in section 2.14 when describing the experimental procedure.

3. The authors showed some numerical data on the fractions of successfully bonded regions and unsuccessful regions. To obtain such statics, how large regions of the grain boundaries were observed and analyzed?
The referee is correct that sufficient statistical data is required to compare the bonded versus non-bonded interface fractions of as-synthesized bicrystals. In this work, bonded interface fractions were calculated from an average grain boundary length of 1.5±0.4 mm. For clarification, we have amended Table 1 in the revised manuscript accordingly.

4. What is the bubble like contrast in the Figure 2a?
Spherical beads observed in Figure 2a represent residual silica from polishing. We have added a clarifying comment to the caption of Figure 2.